Geophysical Research Letters

Supporting Information for

Heat-flow and near-seafloor magnetic anomalies highlight hydrothermal circulation at Brothers volcano caldera, southern Kermadec Arc, New Zealand

Fabio Caratori Tontini[1], Maurice Tivey[2], Cornel E. J. de Ronde[1], and Susan Humphris[2]

1. GNS Science, Lower Hutt, New Zealand
2. Woods Hole Oceanographic Institution, Woods Hole, MA, USA.

Contents of this file

Introduction

This supporting information provides a summary of the processing of the magnetic data (Text S1), of the heat-flow data (Text S2), details of a thermal conductive model and comparison between observed and expected heat-flow anomalies (Text S3).

Text S1 – Magnetic data and processing

Three separate magnetic surveys (Figure S1) were designed to acquire high-resolution geophysical data (Caratori Tontini et al., 2012a; 2012b; Embley et al., 2012) and to examine in detail the discharge of seafloor hydrothermal vents by accurate plume mapping (Baker et al., 2012). The first survey in 2007 consisted of 8 deployments of the AUV *ABE* over the caldera walls and the post-collapse cones. Additional data were collected by the AUV *Sentry* during a single dive in 2011 to map the caldera floor and parts of the resurgent cones. Finally, a detailed survey was carried out in 2018 over the active vent fields at the Upper caldera site using the ROV *Jason*.

The three-component magnetometer data (X, Y, Z) collected during these surveys were transformed into total-intensity by taking the norm of the components. The measured magnetic field was then corrected for remanent and induced field effects originating from the vehicles. This calibration is achieved by fitting the sinusoidal variation of the magnetic field data while the vehicle spins towards

the seafloor (Tivey at al., 2003). Diurnal variation of the magnetic field has not been subtracted from the recorded data because a base station could not be installed close to the survey (e.g., Faggioni and Caratori Tontini, 2002). However, magnetic data from the Eyrewell Intermagnet observatory (Christchurch, New Zealand) show that the survey was performed during magnetically quiet days. The residual magnetic anomaly was obtained by subtracting the International Geomagnetic Reference Field (IGRF) from the total field data (Finlay et al., 2010). The resulting magnetic anomaly data were then interpolated onto a 25-m-spaced grid using a minimum-curvature algorithm. These magnetic anomalies were inverted using the inversion algorithm described in Caratori Tontini et al. (2008) and Caratori Tontini et al. (2012a), using a magnetization direction with inclination -60° and declination 20°, assuming that Natural Remanent Magnetization direction at Brothers volcano is the same of the regional magnetic field (Finlay et al., 2010)

Text S2 – Heat flow data and processing

The heat flow data were collected using a set of thermal blankets (Johnson et al, 2010; Salmi et al., 2014) and the *Alvin* heat-flow probe. The thermal blankets are particularly effective on unsedimented seafloor (hard rocks) and consists of a 5 cm sheet of water-saturated foam with thermistors mounted on the top and bottom of the foam. The conductive thermal gradient is transferred to the water inside the foam where the internal matrix suppresses convection of seawater. For this reason, the thermal conductivity of the blanket is the same for non-convecting seawater. The measured heat flow is then calculated as $\boldsymbol{q = \lambda_w(T_b - T_t)/d}$, where $\boldsymbol{\lambda_w = 0.596\ Wm^{-1}\ K^{-1}}$ is the thermal conductivity of seawater, $\boldsymbol{d}$ is the thickness of the foam sheet (~ 5 cm), $\boldsymbol{T_b}$ and $\boldsymbol{T_t}$ are the asymptotic bottom and top temperature, respectively. The deployment periods varied from a minimum of 9 hours to a maximum of 166 hours (Table S1). The first six hours of the deployment were not included in the calculation of the asymptotic heat flow to remove any influence of the initial heat pulse from previous recovery and redeployment of the thermal blanket to a different location. The asymptotic heat-flow is estimated by plotting the difference in temperature between the two thermistors $\boldsymbol{T_b - T_t}$ vs. 1/time to evaluate the infinite time intercept, i.e. the asymptotic value of $\boldsymbol{T_b - T_t}$. The 0.001°C accuracy of the thermistors limits the heat-flow measurements to a resolution of ±0.01 W/m^2. However, the largest error in the calculation of the heat flow comes from the effects of the near-bottom water temperature variations. The effect of 0.1°C near-bottom water temperature variations over the deployment period of a thermal blanket is ~ 1.2 W/m^2. For this reason, we have estimated the standard error on the heat-flow by using the standard deviation of the near-bottom water temperature during the deployment period (Table S1).

By contrast, the Alvin probe is designed to provide a vertical temperature profile of seafloor sediments. It consists of a titanium tube containing a series of 11 equally-spaced thermistors which are then used to calculate the thermal gradient using a calibrated in situ heat-pulse applied after insertion into the sediments. The heat-flow was obtained by using an average thermal conductivity for the sediments $\boldsymbol{\lambda_s = 0.960\ Wm^{-1}\ K^{-1}}$. Uncertainty in the heat flow estimates arise from instrument sensitivity to measurement uncertainty. The probe thermistors have a 0.001°C resolution and they are fixed within the tube with a 0.1 cm precision. The measurement uncertainty comes in the form of probe depth, which we estimate to be +/- 0.5 cm for a fully inserted probe but greater (perhaps +/-2.5 cm) for a partially inserted probe. The greatest uncertainty is the angle of the probe from vertical as the sensor has no tilt sensor and so is estimated visually. An estimate of this error from duplicate Alvin probe measurements (Salmi, 2018) shows that a tilt error of +/- 26.5 deg provides a conservative approximation of this error. Taken together Salmi (2018) estimates the instrumental heat flow error for the Alvin probe ± 0.02 W/m^2. Another source of uncertainty comes from the Bullard

plot to determine the heat-flow using a linear least-squares fit and the associated standard error. This could be as large as ~ 0.5 W/m^2 depending on the complexity of the gradient curve (Table S1).

In total we collected 52 stations (Table S1), 21 using the thermal blankets (9 during the TN350 cruise and 12 during the SO253 cruise) and 31 using the Alvin heat-flow probe (all of them during the TN350 cruise). Previous authors have investigated the relative comparison between thermal blankets and Alvin probe measurements of heat-flow. These comparisons show general agreement, within 10% as reported by Johnson et al. (2013) and 20% determined by Salmi et al. (2014). In our survey, two stations (HFP1 and C1, see Table S1), located at a distance of ~ 2m were measured using the heat-flow and thermal blanket, one week apart during the TN350 cruise. The measured values were 15.71±0.53 W/m^2 at HFP1 and 25.0±1.2 W/m^2 at C1, respectively. These values were measured in a hot area in proximity to a zone a fluid discharge where significant advection could explain the differences in measured heat-flow at the spatial scale of ~ 2 m.

Text S3 – Thermal conductive model

We derived a conductive thermal model for Brothers volcano to test the hypothesis that heat-transfer is dominated by convection of hydrothermal fluids. The model was developed by using the open KWare Heat3D geophysical heat flow simulator (Wohletz et al., 1999). The model consists of a silicic magma chamber at a depth of ~ 2.5 km, temperature ~ 1000 °C, in a homogeneous crust with average thermal conductivity of 2 W·m^{-1}·K^{-1} (Figure S2).

The model shows that the 100°C isotherm is located at a depth of ~150 m below the caldera floor, deepening to ~ 800 m under the cone and the caldera wall. The calculated surface heat flow shows a broad, bell-shaped pattern with a maximum of ~ 1.3 W/m^2 on the caldera floor and laterally decreases to ~ 0.2 W/m^2 (Figure S3). This is in contrast with the measured heat-flow which shows high spatial variability with minimum heat-flow on the caldera floor and maxima in coincidence hydrothermal fields on the NW caldera and Cone sites. This suggests that hydrothermal convection is the main mechanism of heat-transfer at Brothers volcano.

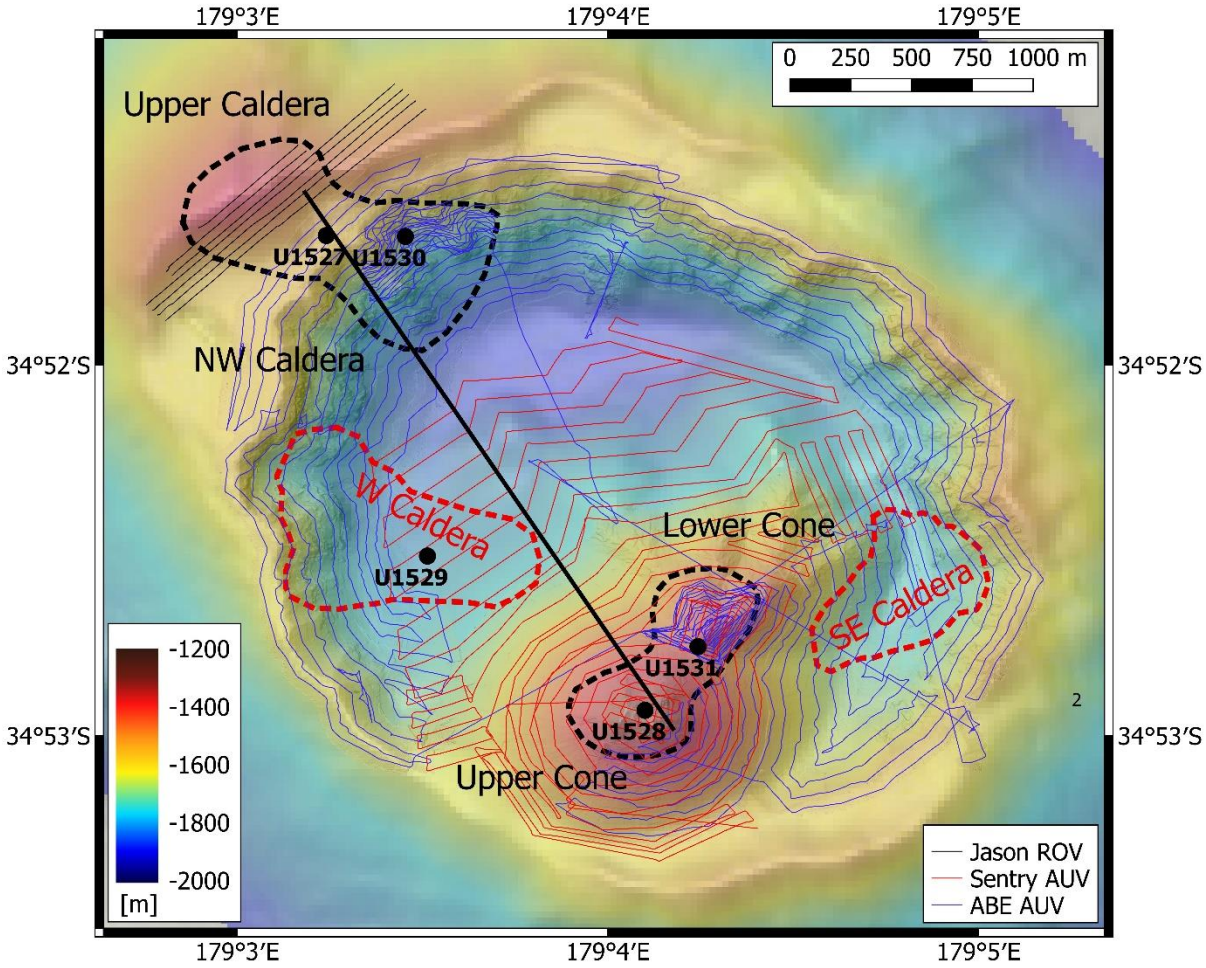

Figure S1. Magnetic survey lines at Brothers volcano, locations and extent of Upper and Lower Cone and Upper and NW Caldera hydrothermal sites (black dashed polygons), W caldera and SE caldera hydrothermal sites (red dashed polygons). International Ocean Discovery Program (IODP) sites U1527, U1528, U1529, U1530 and U1531 are drill-sites discussed in the text. Heat-flow modelled profile (black line) of Figure S2 and S3 in proximity to the seismic line Bro-3 shown in de Ronde et al. (2017).

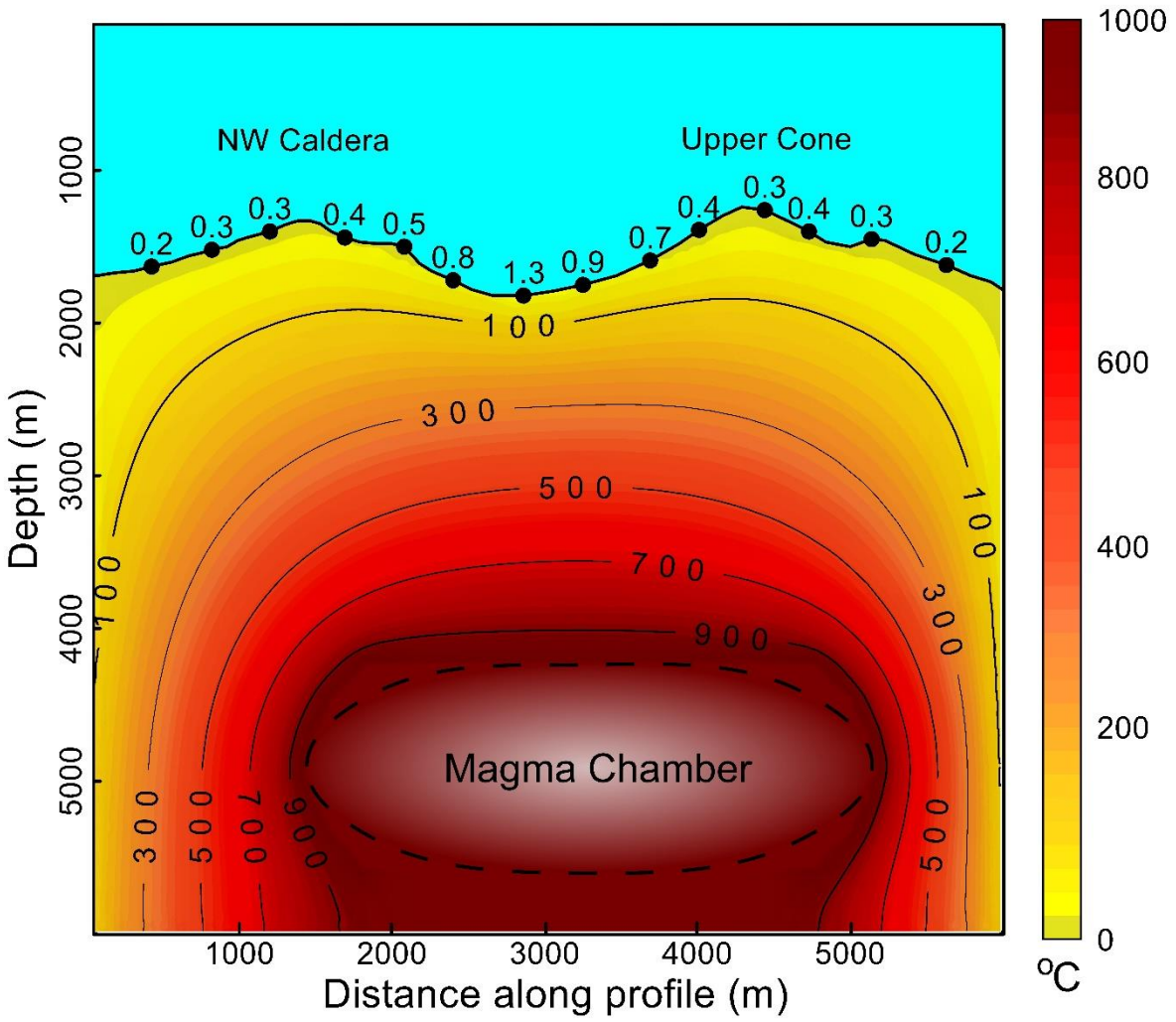

Figure S2. Thermal conductive model including a silicic magma chamber at ~2.5 km depth below sea floor with a magma temperature 1000 °C and average thermal conductivity of 2 $W \cdot m^{-1} \cdot K^{-1}$ for the crust. Posted numbers represent the expected heat-flow [$W \cdot m^{-2}$] at specific surface locations.

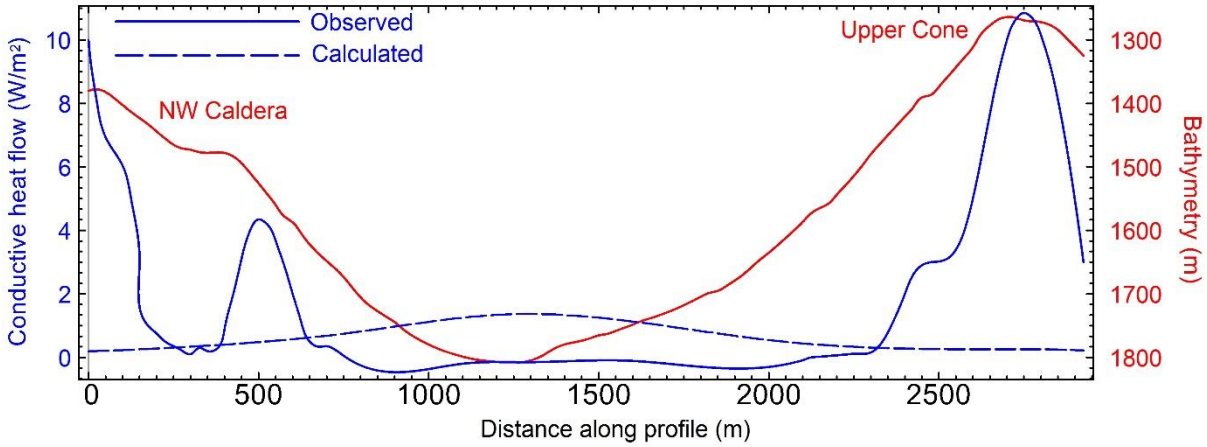

Figure S3. Comparison between observed and calculated conductive heat-flow along the line shown in Figure S1 using the model of Figure S2.

Station	Latitude	Longitude	Heat Flow	Error	Note
HFP1	-34.8589	179.0496	15.71	0.53	100% penetration
HFP2	-34.8615	179.0515	-0.12	0.02	100% penetration
HFP3	-34.8751	179.0586	-0.07	0.02	20% penetration
HFP4	-34.8654	179.0580	3.59	0.14	100% penetration
HFP5	-34.8703	179.0583	-0.14	0.02	70% penetration
HFP6	-34.8788	179.0623	-0.3	0.08	30% penetration
HFP7	-34.8789	179.0662	-0.14	0.01	30% penetration
HFP8	-34.8818	179.0656	6.16	0.42	100% penetration
HFP9	-34.8821	179.0678	3.44	0.2	100% penetration
HFP10	-34.8821	179.0685	-0.08	0.02	100% penetration
HFP11	-34.8827	179.0687	24.16	N/A	10% penetration, only one sensor inserted
HFP12	-34.8807	179.0697	0.08	0.02	100% penetration
HFP13	-34.8729	179.0672	-0.02	0.02	100% penetration, complex gradient
HFP14	-34.8752	179.0716	-0.15	0.02	80% penetration
HFP15	-34.8775	179.0690	0.48	0.07	75% penetration
HFP16	-34.8788	179.0710	8.78	0.1	80% penetration
HFP17	-34.8757	179.0748	0.1	0.02	50% penetration
HFP18	-34.8759	179.0809	-0.06	0.02	100% penetration
HFP19	-34.8709	179.0744	-0.09	0.02	100% penetration
HFP20	-34.8651	179.0727	0.74	0.05	66% penetration
HFP21	-34.8617	179.0759	0.4	0.02	100% penetration
HFP22	-34.8605	179.0683	1.58	0.08	66% penetration
HFP23	-34.8601	179.0611	-0.19	0.07	66% penetration
HFP24	-34.8618	179.0578	40.61	0.7	50% penetration
HFP25	-34.8626	179.0566	16.26	0.39	85% penetration
HFP26	-34.8634	179.0555	1.73	0.12	75% penetration
HFP27	-34.8630	179.0574	8.77	0.24	85% penetration
HFP28	-34.8665	179.0609	-0.1	0.02	100% penetration
HFP29	-34.8626	179.0599	-0.04	0.02	100% penetration, complex gradient
HFP30	-34.8608	179.0598	17.28	0.58	100% penetration
HFP31	-34.8578	179.0595	0.66	0.02	100% penetration
F4	-34.8775	179.0716	20.3	2.7	~ 21 hours, SO253 cruise
F5	-34.882	179.0684	0.2	1.8	~ 66 hours, SO253 cruise
F6	-34.8821	179.0683	0.7	2.4	~ 96 hours, SO253 cruise
G4	-34.8786	179.0707	13.0	2.5	~ 23 hours, SO253 cruise
G5	-34.8818	179.0687	66.3	2.1	~ 23 hours, SO253 cruise
G6	-34.8608	179.054	0.6	1.8	~ 30 hours, SO253 cruise
H3	-34.8785	179.071	125.4	3.6	~ 21 hours, SO253 cruise
H4	-34.8831	179.0696	1.7	2.0	~ 48 hours, SO253 cruise
H5	-34.8607	179.0546	0.0	1.8	~ 51 hours, SO253 cruise
I3	-34.8791	179.0704	16.0	2.8	~ 21 hours, SO253 cruise
I4	-34.8795	179.0705	-0.1	1.3	~ 46 hours, SO253 cruise
I5	-34.8606	179.0554	0.6	1.5	~ 48 hours, SO253 cruise
A1	-34.8601	179.0533	0.0	0.8	~ 144 hours, TN 350 cruise
A2	-34.8574	179.0523	10.2	1.5	~ 20 hours, TN 350 cruise
B1	-34.8593	179.0522	14.7	1.0	~ 142 hours, TN 350 cruise
B2	-34.8583	179.0508	-0.8	1.2	~ 21 hours, TN 350 cruise
C1	-34.8589	179.0496	25.0	1.2	~ 168 hours, TN 350 cruise
C2	-34.8622	179.0538	-0.9	0.3	~ 12 hours, TN 350 cruise
D1	-34.8615	179.0557	0.1	0.8	~ 166 hours, TN 350 cruise
D2	-34.8608	179.0487	0.3	0.3	~ 13 hours, TN 350 cruise
E2	-34.8608	179.0572	32.7	N/A	~ 9 hours, TN 350 cruise, bottom water temperature estimated

Table S1. Heat-flow data. Stations starting with HFP are Alvin probe data. Latitude and Longitude in decimal degrees, heat flow in W/m^2. Error estimated from Bullard plots and instrumental heat-flow error of 0.02 W/m^2 for the Alvin probe, and bottom-water temperature variability for the thermal blankets. Notes reporting the penetration of the Alvin probe and duration of the thermal blankets deployments.

References

Baker, E. T., R. W. Embley, C. E. J. de Ronde, and S. Walker (2012), High-resolution hydrothermal mapping of Brothers caldera, Kermadec arc, Econ. Geol., 107, 1583–1593, doi: 10.2113/econgeo.107.8.1583

Caratori Tontini, F., L. Cocchi, and C. Carmisciano (2008), Potential-field inversion for a layer with uneven thickness: the Tyrrhenian Sea density model, Phys. E. Plan. Int., 166, 105-111

Caratori Tontini, F., B. Davy, C. E. J. de Ronde, R. W. Embley, M. Leybourne, and M. A. Tivey (2012a), Crustal magnetization of Brothers Volcano, New Zealand, measured by autonomous underwater vehicles: Geophysical expression of a submarine hydrothermal system, Econ. Geol., 107, 1571–1581.

Caratori Tontini, F., C. E. J. de Ronde, D. Yoerger, J. C. Kinsey, and M. A. Tivey (2012b), 3-D focused inversion of near-seafloor magnetic data with application to the Brothers Volcano hydrothermal system, Southern Pacific Ocean, New Zealand, J. Geophys. Res., 117, B10102, doi:10.1029/2012JB009349.

Embley, R. W., C. E. J. de Ronde, S. G. Merle, B. Davy, and F. Caratori Tontini (2012), Detailed morphology and structure of an active submarine arc caldera: Brothers Volcano, Kermadec arc, Econ. Geol., 107(8):1557– 1570.

Faggioni, O., and F. Caratori Tontini (2003), Quantitative evaluation of the time-line reduction performance in high definition marine magnetic surveys, Mar. Geophys. Res., 23, 353-365.

Johnson, H. P., M. A. Tivey, T. A. Bjorklund, and M. S. Salmi (2010), Hydrothermal circulation within the Endeavour Segment; Juan de Fuca Ridge, Geochem. Geophys. Geosyst., 11, Q05002, doi:10.1029/2009GC002957.

Salmi, M. S., H. Paul Johnson, M. A. Tivey, and M. Hutnak (2014), Quantitative estimate of heat flow from a mid-ocean ridge axial valley, Raven field, Juan de Fuca Ridge: Observations and inferences, J. Geophys. Res. Solid Earth, 119, doi:10.1002/2014JB011086.

Salmi, M.S., (2018). The Thermal and Fluid Environment of the Cascadia Subduction Zone, Southern Washington State, PhD. Thesis, University of Washington, pp 176.

Tivey, M. A., H., Schouten, and M. C. Kleinrock, 2003, A near-bottom magnetic survey of the Mid-Atlantic Ridge axis at 26° N: Implications for the tectonic evolution of the TAG segment: Journal of Geophysical Researches, v. 108, p. 2277, doi:10.1029/2002JB001967.

Wohletz, K., L. Civetta, and G. Orsi (1999), Thermal evolution of the Phlegraean magmatic system, J. Volcanol. Geotherm. Res., 91, 381–414